Published in final edited form as:
Cell Calcium. 2013 August ; 54(2): 57–70. doi:10.1016/j.ceca.2013.04.004.

Ca^{2+} signaling in human induced pluripotent stem cell-derived cardiomyocytes (iPS-CM) from normal and catecholaminergic polymorphic ventricular tachycardia (CPVT)-afflicted subjects

X.-H. Zhang[a], **S. Haviland**[a], **H. Wei**[a], **T. Šarić**[b], **A. Fatima**[b], **J. Hescheler**[b], **L. Cleemann**[a], and **M. Morad**[a,*]

[a]Cardiac Signaling Center of USC, MUSC, & Clemson University, Charleston, SC, USA

[b]Institute for Neurophysiology, Medical Center, University of Cologne, Cologne, Germany

Abstract

Derivation of cardiomyocytes from induced pluripotent stem cells (iPS-CMs) allowed us to probe the Ca^{2+}-signaling parameters of human iPS-CMs from healthy- and catecholaminergic polymorphic ventricular tachycardia (CPVT1)-afflicted individuals carrying a novel point mutation p.F2483I in ryanodine receptors (RyR2). iPS-CMs were dissociated on day 30–40 of differentiation and patch-clamped within 3–6 days. Calcium currents (I_{Ca}) averaged ~8 pA/pF in control and mutant iPS-CMs. I_{Ca}-induced Ca^{2+}-transients in control and mutant cells had bell-shaped voltage-dependence similar to that of I_{Ca}, consistent with Ca^{2+}-induced Ca^{2+}-release (CICR) mechanism. The ratio of I_{Ca}-activated to caffeine-triggered Ca^{2+}-transients was ~0.3 in both cell types. Caffeine-induced Ca^{2+}-transients generated significantly smaller Na^{+}–Ca^{2+} exchanger current (I_{NCX}) in mutant cells, reflecting their smaller Ca^{2+}-stores. The gain of CICR was voltage-dependent as in adult cardiomyocytes. Adrenergic agonists enhanced I_{Ca}, but differentially altered the CICR gain, diastolic Ca^{2+}, and Ca^{2+}-sparks in mutant cells. The mutant cells, when Ca^{2+}-overloaded, showed longer and wandering Ca^{2+}-sparks that activated adjoining release sites, had larger CICR gain at −30 mV yet smaller Ca^{2+}-stores. We conclude that control and mutant iPS-CMs express the adult cardiomyocyte Ca^{2+}-signaling phenotype. RyR2 F2483I mutant myocytes have aberrant unitary Ca^{2+}-signaling, smaller Ca^{2+}-stores, higher CICR gains, and sensitized adrenergic regulation, consistent with functionally altered Ca^{2+}-release profile of CPVT syndrome.

Keywords

Mutation in RyR2 gene; Pluripotent stem cells; CPVT; Calcium signaling; CICR gain

1. Introduction

Recent breakthroughs in stem cell biology have made it possible to develop pluripotent stem cells from adult fibroblasts by transfecting them with a set of 4 “stemness” genes (inducible

*Corresponding author at: Cardiac Signaling Center of University of South Carolina, Medical University of South Carolina and Clemson University, MUSC, 68 President Street, BEB 306 Charleston, SC 29403, USA. Tel.: +1 843 876 2400; fax: +1 843 792 4606; mobile: +1 803 873 7113. moradm@musc.edu (M. Morad).

Conflicts of interest
We have no conflicts of interest.

Disclosures
None.

pluripotent stem cells, iPSC, [1]). This reprogramming allows experimental approaches that drive such cells to acquire cardiac molecular and electrophysiological phenotypes [2–4], thus creating opportunities for therapy of a host of cardiac pathologies using patient-derived cells. This approach has made it also possible to examine patient-specific mutations in ion channels and Ca^{2+} signaling proteins that might lead to arrhythmia and heart failure in iPS-CM in a laboratory setting, thus devising pharmacological patient-specific paradigms for therapy [5–11]. In light of such potentials, it is imperative that the electrophysiological and Ca^{2+} signaling properties of human iPS-CM as well as their pharmacology are fully identified and quantified.

Ca^{2+}-signaling in mammalian hearts is characterized by: (1) I_{Ca}-gated Ca^{2+}-release (CICR), providing for the characteristic bell-shaped voltage-dependence of Ca^{2+} transients that closely reflect the voltage-dependence of I_{Ca}; (2) the gain of CICR is voltage-dependent, not predicted from a strictly Ca^{2+}-dependent process [12–14]; (3) β-adrenergic agonists enhance I_{Ca}, Ca^{2+} content of the sarcoplasmic reticulum (SR), Ca_i-transients and accelerate their decay kinetics, consistent with PKA-mediated phosphorylation of DHPRs, phospholamban/SERCA2a complex, and the RyR2; (4) Caffeine-triggered Ca^{2+}-release activates an inward current (I_{NCX}) with time-course and kinetics similar to rise and fall of cytosolic Ca^{2+}, reflecting the efflux of Ca^{2+} on the electrogenic Na^+–Ca^{2+} exchanger (NCX). Although there are already a number of reports on the electrophysiology of iPS-CM [15–17] there are few detailed reports on their Ca^{2+} signaling pathways and their regulation beyond measurements of Ca^{2+} transients in intact non-voltage clamped cells [9,18] and in embryonic stem cell-derived cardiomyocytes [19].

In this report, we describe the Ca^{2+} signaling properties of human iPS-CM by quantifying the activities of Ca^{2+}-signaling proteins that include the density, kinetics, and regulation of Ca^{2+} channels and NCX transporter, the size of SR Ca^{2+}-stores, its regulation by β-adrenergic agonists, the voltage-dependence of I_{Ca} and Ca^{2+}-transients, the gain of CICR, the efficiency of Ca^{2+}-release mechanism, and the properties of the individual dyadic calcium release (sparks). In addition, we have attempted to quantify possible abnormalities in these parameters in cells derived from a patient afflicted with catecholaminergic polymorphic ventricular tachycardia (CPVT), carrying a recently identified ryanodine receptor mutation (p.F2483I) [9]. Our data suggests that Ca^{2+}-signaling properties of adult cardiac myocytes are closely replicated in human iPS-CM. That is, I_{Ca}-gated SR Ca^{2+}-release is the primary mechanism for the release of Ca^{2+} on depolarization of the cell by the action potential. Relaxation, in a manner similar to mammalian myocardium, is mediated by reuptake of Ca^{2+} into the SR and extrusion of Ca^{2+} by the Na^+–Ca^{2+} exchanger, producing currents often in excess of 2–3 pA/pF. While adrenergic agonists strongly enhanced I_{Ca}, and accelerated the rate of decay of the Ca^{2+}-transients, they had insignificant effects on NCX currents, consistent with findings in adult mammalian hearts [20,21]. These findings led us to conclude that human iPS-CM represent a reliable Ca^{2+}-signaling model of mammalian cardiomyocytes.

Numbers of recent reports have implicated RyR2-mutations and the resultant abnormal Ca^{2+} signaling in development of arrhythmia and sudden death associated with intense adrenergic stimulation in patients with CPVT. It has been proposed that such mutation renders the RyRs “leaky” on exposure to β-adrenergic agonists (hyperphosphorylation & dissociation of calstabin from RyR2, [22,23] producing localized increases in Ca^{2+} that is extruded on NCX generating local depolarization (EADs & DADs), triggering at times fatal arrhythmias. Alternatively, overloading of SR Ca^{2+}-stores by adrenergic agonists has been proposed [24,25] to lead to increased probability of RyR2 channel openings, resulting in abnormal release of Ca^{2+} and the resultant membrane-depolarization and arrhythmias. These ideas have been tested in a number of knock-in mice and *in vitro* models [26–29], but their

validity in the human disease remain still somewhat clouded by both the variability of the RyR2 point mutations producing CPVT, the locus of phosphorylation on RyR2, lack of universal confirmatory results, and absence of clear-cut pharmacology [25].

Our data here suggests that despite significant quantitative intercellular differences in Ca^{2+}-signaling parameters of control and RyR2 mutant cells, they both had equivalent and elevated densities of Ca^{2+} currents and NCX activity, similar bell-shaped voltage-dependence of I_{Ca}-gated Ca^{2+}-release, and voltage-dependent CICR gain. Mutant cells, however, were consistently found to have smaller caffeine-triggered Ca^{2+}-stores higher CICR gain, especially at −30 mV, consistent with longer, recurrent and often wandering Ca^{2+}-sparks, compared to sporadic and brief sparks of control iPS-CM. Though adrenergic agonists produced equivalent and large enhancements of I_{Ca} in both mutant and control cells, they differentially altered the CICR gain, diastolic Ca^{2+}, and Ca^{2+}-sparks in mutant cells consistent with aberrant Ca^{2+}-release profiles of Ca^{2+}-overloaded CPVT-mutant myocytes, and the higher proclivity for generation of DADs and EADs in mutant hearts.

2. Methods

2.1. Cultivation of human iPS cells and preparation of cardiomyocytes

2.1.1. Culture of undifferentiated human iPS cells—The human iPS cell lines were derived from dermal fibroblasts of a CPVT-afflicted patient carrying a *de novo* heterozygous autosomal dominant p.F2483I mutation in RYR2 and a healthy subject. The generation, cardiac differentiation and characterization of these cell lines were reported recently [9]. The iPS cells were maintained on mitomycin C treated murine embryonic fibroblasts (MEF) prepared in our laboratory in DMEM/F12 medium supplemented with Glutamax, 20% knockout serum replacer, 1% nonessential amino acids (NAA), 0.1 mM β-mercaptoethanol (βME, Invitrogen, Darmstadt, Germany), 50 ng/ml FGF-2 (PeproTech, Hamburg, Germany). Cells were passaged by manual dissection of cell clusters every 5–6 days.

2.1.2. Cardiac differentiation—Cardiac differentiation of human iPS cells was carried out on the murine visceral endoderm-like cell line (END_2), which was provided by C. Mummery (Leiden University Medical Center, The Netherlands). END_2 cells were mitotically inactivated for 3 h with 10 μg/ml mitomycin C (Sigma–Aldrich Chemie GmbH, Munich, Germany) and 1.2×10^6 cells were plated on 6 cm dishes coated with 0.1% gelatin one day before initiation of iPS cell differentiation. To initiate co-cultures, iPS cell colonies were dissociated into clumps by using collagenase IV (Sigma-Aldrich, 1 mg/ml in DMEM/F-12 at 37 °C for 5–10 min). The differentiation was carried out in 1% knockout-DMEM containing 1 mM L-glutamine, 1% NAA, 0.1 mM βME and 1% penicillin/streptomycin (100 U/ml and 100 μg/ml, respectively). The co-culture was left undisturbed at 37 °C/5% CO_2 for 5 days. First medium change was performed on day 5 and later on days 9, 12 and 15 of differentiation. Spontaneously contracting clusters were dissociated into single cardiomyocytes for experiments.

2.1.3. Preparation of iPS-CM for patch-clamp experiments—Beating areas were micro-dissected mechanically at day 30–40 of differentiation, dissociated with collagenase B, and single iPS-CM then plated on fibronectin (2.5 μg/ml)-coated glass coverslips in 6 well plates. Cells were incubated for 36–72 h before their use in electrophysiological experiments.

2.2. Measurements of cellular currents and global Ca^{2+}

iPS-CM were voltage-clamped in the whole-cell configuration. L-type Ca^{2+} current (I_{Ca}) and I_{NCX} were activated by depolarizing pulses or exposure to caffeine. The voltage-clamped cells were dia-lyzed with a Cs^+-based, moderately Ca^{2+}-buffered pipette solution containing (in mM): 110 Cs^+-Aspartate, 15 or 5 NaCl, 20 TEACl, 5 Mg-ATP, 0.2 EGTA and 0.1 Fluo-4 pentapotassium, 0.1 $CaCl_2$ ($[Ca^{2+}]_i \sim 100$ mM), 10 glucose and 10 HEPES (titrated to pH 7.2 with CsOH; measured osmolarity: 295 mOsm) allowing simultaneous measurements of intracellular Ca^{2+} transients. L-type Ca^{2+} current (I_{Ca}) was measured by depolarization to 0 mV from a holding potential of −50 or −40 mV using a Dagan amplifier and pClamp (Clampex 10.2) software. Borosilicate patch pipettes were prepared using a horizontal pipette puller (Model P-87, Sutter Instruments, CA). The pipettes had a resistance of 3–5 MΩ. The extracellular solution in the experimental chamber contained (in mM): 137 NaCl, 5.4 KCl, 2 $CaCl_2$, 1 $MgCl_2$, 10 glucose and 10 HEPES (titrated to pH 7.4 with NaOH). To facilitate recordings of I_{Ca} and I_{NCX}, we blocked K^+ currents, not only by including TEA in the dialyzing solution, but also by using an electromagnetically controlled puffing system that applied K^+-free solutions in the immediate vicinity of the voltage-clamped cell. I_{Ca} was modulated by adding isoproterenol or Bay-K 8644 to the K^+-free puffing solutions while rapid application of 3 mM caffeine was used to probe the magnitude of SR Ca^{2+} stores and activate I_{NCX}. I_{Ca} was normalized relative to the membrane capacitance and plotted in units of pA/pF. All experiments were carried out at room temperature (22–24 °C).

Cellular Ca^{2+} transients in voltage-clamped cells were measured fluorometrically by including 0.1 mM Fluo-4 pentapotassium salt in the dialyzing pipette solution. The dye was excited by 460 nm light from a LED-based illuminator (Prismatix, Modiin Ilite, Israel) and Ca^{2+}-dependent fluorescent light (>500 nm) was detected with a photomultiplier tube that placed behind a moveable, adjustable diaphragm, which served to limit the area of detection to the voltage-clamped cell. The cellular fluorescence signals ($\Delta F/F_0$) were normalized by dividing the changes in whole-cell fluorescence (ΔF) with the baseline fluorescence (F_0).

2.3. Ca^{2+} imaging measurements

2.3.1. TIRF imaging and analysis of ratiometric images—Single isolated beating cardiomyocytes derived from iPS cells were plated on non-coated WillCodish, glass bottom Petri dishes (Ted Pella Inc., 35 × 10 mm, 22 mm glass) and allowed to attach for three days before imaging. Intracellular Ca^{2+} signals were measured with the fluorescent Ca^{2+}-indicator dye Fluo-4AM (5 μM, Invitrogen) after 30 min incubation at 37 °C and 5% CO_2. The cells were imaged using a Leica multicolor total internal reflection fluorescence (TIRF) imaging system (Leica Microsystems, Buffalo Grove, IL) fitted with a 63× oil-immersion objective lens and an Andor iXon3 camera with 512 × 512 pixels. An argon ion laser was used for excitation at 488 nm and fluorescence emission was measured at wavelengths >515 nm. Cells were imaged at 70–100 Hz with a depth of penetration less than 200 nm into the cell and focus on sub-sarcolemmal Ca^{2+} release in regions where the cell membrane was attached to the underlying glass cover slips. The pixel size in the object plane was 0.25 μm square, or 0.157 μm with 1.6 zoom [30,31]. Images were binned using 2×2 pixel averaging. The external bath solution contained (in mM): 137 NaCl, 4 KCl, 10 HEPES, 10 Glucose, 1 $MgCl_2$, 2 $CaCl_2$ with pH 7.4 using NaOH. Sparks were measured in control *vs.* CPVT-iPS-CM in control bath solution and in response to 3 min application of 100 μM 8-Br-cAMP.

The obtained image sequences were collected and surveyed with Leica software (LAS AF), but displayed and analyzed in detail using a custom-designed program (Con2i). The method of analysis is illustrated in Fig. 1. Initially each frame was subjected to 2 × 2 or 3 × 3 pixel averaging. This was followed by scaling that equalized the fluorescence intensity throughout

the diastolic intervals (Panel A). An average diastolic image (AVE, $F_0(x,y)$, Panel B) was then calculated based on a large number of selected diastolic images with little or no indication of Ca^{2+} release activity. Such averaged images showed the footprints of the examined cells that typically had well defined outlines around regions of stable attachment where the fluorescence intensity varied significantly. This variability may reflect the stationary distribution of intracellular organelles and some undulation of the cell membrane and extracellular matrix. To compensate for the stationary variability each frame was divided by the average (#380/AVE, $F(x,y,t)/F_0(x,y)$, Panel B). The resulting ratiometric images showed a fairly uniform intensity as a mottle of dark blue hues which extended throughout the cell except for hotspots of focal Ca^2 release activity that were displayed in warmer colors of green, yellow, orange and red (arrows). Panel C shows a sequence of frames (#28–43) where a Ca^{2+} spark first appeared abruptly as a small bright spot (~1 μm across, frame #29) that grew in size (#30–33) and flared up at a slightly different location (#34) before it finally faded and disappeared (#43). The time course of each Ca^{2+} sparks could be follow by defining a region of interest based on its first appearance (see Figs. 7, 9 and supplement 1). This approach was used to evaluate the duration of Ca^{2+} sparks as the intervals where the intensity exceeded 50% of the peak value (Fig. 7C). To chart the evolution of Ca^{2+} sparks and detect shifts from one release site to another, we also used an algorithm that approximated each image of local Ca^{2+} release with a Gaussian distribution (Panel D) and followed changes in location, amplitude, variance and helicity from frame to frame. This approach allowed the location of Ca^{2+} release sites to be determined with an accuracy of 0.1–0.3 μm depending on the signal-to-noise ratio.

2.3.2. Confocal Ca^{2+} imaging—Voltage-clamped iPS-CM dialyzed with fluorescent and non-fluorescent Ca^{2+} buffers (0.2 mM Fluo-4, 0.5 mM EGTA, with 0.5 mM Ca^{2+}) were imaged at a frame rate of 120–240 Hz on a Noran Odyssey confocal microscope as previously described [31]. The focal plane was adjusted to the midsection of the cell intersecting its nuclei.

2.4. Confocal immuno-fluorescence imaging of RyR2 distributions

Immuno-labeled RyR2 in fixed iPS-CMs were imaged on a Leica confocal microscope following published procedures [32], but using a primary antibody to RyR2 (1:100 anti RyR Mab by Thermo Scientific). Briefly, immunocytochemical approaches were used to detect RyR2 in cultures of control, IMRC8 iPSC-CM. Media was removed and cells were rinsed with phosphate-buffered saline (PBS), and then fixed with ice cold methanol for 10 min. After washing the cells with PBS, the cells were blocked in 1% bovine serum albumin and 0.1% Triton in PBS. Then the blocking solution was removed, and primary antibody (1:100 anti RyR Mab by Thermo Scientific) was applied overnight at 4 °C in block. After washing out the cells 3 times with PBS, anti-mouse FITC (1:100) in block was applied for 2 h at room temperature. The secondary antibody dilution was removed, washed, and the cover slip was mounted on a slide using a drop of ProLong Gold with DAPI and allowed to cure for 24 h at room temperature and stored at −20 °C. Imaging was performed on a Leica TCS SPS AOBS confocal microscope system using a 488 nm argon ion laser to examine FITC expression of RyR2 and a 405 nm diode laser to examine nuclear DAPI expression using a 63× oil objective with zoom function.

2.5. Statistical analysis

Average values are presented in histograms and in the text as the mean ± the standard error of the mean for "*n*" cells. The distribution of data in individual cells is shown in separate panels. *T*-test was used to determine statistical significance. Significant findings are labeled with one ($p < 0.05$, *) or two stars ($p < 0.01$, **).

3. Results

3.1. Calcium current in iPS-CM from healthy and CPVT subjects

Cardiomyocytes from two control human iPS cell lines (clones 5 (C5) and 8 (C8)) and one CPTV iPS cell line (clone 1, NP0014-C1)) were used in the comparative electrophysiological and Ca^{2+}-signaling experiments. To approximate as closely as possible, the internal media of intact contracting cells, I_{Ca} was measured in cells dialyzed with low Ca^{2+}-buffered solutions (in mM: 0.2 EGTA, 0.1 Fluo4, 0.1 Ca^{2+}, see Section 2), containing either 5 or 15 mM Na^+. Fig. 2D, shows that I_{Ca} averaged about 8 pA/pF in control and mutant cells, in bathing solutions containing 2 mM Ca^{2+}, with significant distribution in I_{Ca} density between individual cells of three cell lines (Fig. 2A). The variability in the current density could not be attributed solely to the age of cells in culture nor to cell size (cell capacitance, indicated at the bottom of each column) or intracellular Na^+ concentrations (Panels B and D).

The time course of inactivation of I_{Ca} in low Ca^{2+}-buffered dialyzing solutions was best fit with two exponentials (tau_{fast} = ~10 ms, and tau_{slow} = ~60 ms, Fig. 2C). Increasing the intracellular Na^+ from 5 to 15 mM had little effect on the magnitude or kinetics of I_{Ca}. Mostly, spontaneously beating single cells were selected for Ca^{2+} signaling experimentations.

3.2. I_{Ca}-gated Ca^{2+}-release

Fig. 3A and B compares the voltage-dependence of I_{Ca} and the accompanying Ca_i-transients in representative control and mutant cells. In a manner similar to that observed in mammalian myocardium for developed tension and Ca_i-transients [33–35], a bell-shaped voltage-dependence was found for both parameters that activated at −30 mV, peaked at ~0–10 mV and decreased back to baseline levels between +60 and +80 mV (middle panels in Fig. 3A and B). I_{Ca} reactivated on repolarizations from positive potentials (+60 to +80 mv) also triggered Ca^{2+}-release (inset traces, Panels A and B) as was first described for the rat ventricular myocytes [34]. This strict dependence of Ca^{2+}-transients on I_{Ca} and not on the direction of voltage change, is considered as phenotypic cardiac EC-coupling characteristic, distinguishing cardiac from skeletal muscle that is primarily regulated by voltage-induced Ca^{2+}-release (VICR) mechanism [33–35]. The findings of Fig. 3A and B suggest that human iPS-CMs express only the cardiac-type EC-coupling. Although there was considerable variability as to the degree of development of the maintained components of Ca_i-transients in both mutant and control cell lines, Ca_i-transients always decreased at positive potentials and activated Ca_i-transients on repolarizations from these potentials (60–80 mV, inset traces, Fig. 3A and B). Comparison of control and mutant cells did not reveal significant differences in the rate of activation and decay or the voltage dependence of I_{Ca}-gated Ca_i-transients, suggesting no apparent global EC-coupling defects resulting from p.F2483I RyR2 point mutation under baseline conditions.

Confocal spatial imaging of I_{Ca}-triggered Ca^{2+} release of Fig. 3C–E shows that Ca^{2+} release within the first 25 ms of depolarization occurred primarily near the cell surface membrane before rising in the interior cytoplasmic space. Fig. 3C shows the typical representation of the rounded appearance of a bi-nucleated (*n*, *n*) voltage-clamped Fluo-4 dialyzed iPS-CM, where step-depolarization produced regional Ca^{2+} signals that developed more quickly around the perimeter of the cell (red trace in Fig. 3C representing the red mask of Fig. 3D) than in its deeper layers (orange, green) or nuclei (blue). The release of Ca^{2+} from superficial SR Ca^{2+} stores is consistent with Fig. 3F, showing an immuno-fluorescence distribution of RyRs in a cluster of iPS-CMs suggesting punctate clustering of RyR2s near the surface membrane. These distributions are reminiscent of adult atrial or immature

ventricular cardiomyocytes [36], but differ from those of adult ventricular cells where synchronous activation is supported by a t-tubular network [31] as occasionally observed in a small subset of iPS-CM (Suppl. Fig. 2).

3.3. SR Ca^{2+}-stores

3.3.1. Fractional Ca^{2+}-release—Fractional Ca^{2+}release, in the context of this study, is defined as the ratio of I_{Ca}- to caffeine-triggered Ca_i-transients. This ratio is generally close to unity (0.6–0.9) in adult mammalian ventricular cells under our Ca^{2+} loading conditions, but significantly lower (<0.4) in atrial cells or with reduced Ca^{2+} loading of the SR [37,38]. Since Ca^{2+} release in cardiac myocytes depends on the magnitudes of both I_{Ca} and Ca^{2+} stores, the ratio of Ca^{2+} released by I_{Ca} and caffeine (representing near-full release) may be taken as the effectiveness of Ca^{2+}channel-gated release. Fig. 4 quantifies the fractional Ca^{2+} release in control and mutant myocytes dialyzed with 5 or 15 mM Na^+ (Fig. 4C). The higher intracellular concentrations of Na^+ used in the low Ca^{2+}-buffered pipette solutions are thought to increase the myocyte Ca^{2+}-load [35]. The fractional release averaged ~0.3, in control and mutant cells (Fig. 4C), with some cells showing ratios as high as 0.6 and 0.9 (Fig. 4A and B). The fractional release was not significantly altered in 15 mM Na^+ dialyzed cells in either control or mutant cells (Panel C). Fig. 4D shows representative traces of Ca_i-transients activated by I_{Ca} or triggered by caffeine recorded in control and RyR2-mutant myocytes, (upper and lower traces, respectively).

3.3.2. SR calcium load—To quantify the magnitude of SR Ca^{2+} stores iPS-CMs were subjected to rapid puffs of caffeine containing solutions. In whole-cell patch-clamped iPS-CMs caffeine applications produced large transient rises in the global Ca^{2+} accompanied by activation of large inward I_{NCX}. Fig. 5A and B represents tracings of the time course of caffeine-triggered Ca_i-transients and I_{NCX} in control and CPVT-mutant cells. Although there was significant variability in the magnitude of caffeine-triggered Ca^{2+} release between individual cells within control (Panel C) and mutant (Panel D) cell lines, on average, there was markedly smaller caffeine-triggered Ca^{2+}release in mutant compared to control cells (Panel E), suggesting significantly smaller SR Ca^{2+} stores in the mutant cells. Consistent with this idea, the Na^+–Ca^{2+} exchanger current (I_{NCX}) representing the electrogenic extrusion of Ca^{2+}, as cytosolic Ca^{2+} rises by caffeine-triggered Ca^{2+} release, was also significantly larger (~2.2 pA/pF) in control compared to the mutant cells (~1.5 pA/pF) suggesting smaller caffeine-triggered Ca^{2+}-stores in mutant cells. The time course of Ca^{2+} rise and fall was also quite variable in different cells, but there was no consistent change in the duration of the release or its relaxation rate between control and mutant cells.

Fig. 5F quantifies the rise in cytosolic Ca^{2+} as measured by the integral of I_{NCX} activated by caffeine-triggered Ca^{2+} release in control and mutant cells as the cellular Na^+ load was increased from 5 to 15 mM. This procedure enhances the entry of Ca^{2+} on NCX leading to increased Ca^{2+}-load of the SR. Note that increasing Na^+ from 5 to 15 mM enhanced only slightly the Ca^{2+} load of the SR in control cells. In sharp contrast, however, the elevation of $[Na^+]_i$ in mutant myocytes increased significantly the Ca^{2+} load of the SR. This proclivity to Ca^{2+} loading in mutant myocytes may contribute to leakiness of SR and arrhythmogenesis under the *in vivo* conditions where mutant RyR2 would become more susceptible in causing localized releases of Ca^{2+} and activation of early and delayed after-depolarization (EADs and DADs).

3.3.3. Gain of I_{Ca}-gated Ca^{2+}-release—The degree to which I_{Ca} triggers Ca^{2+} release normalized for the Ca^{2+} content of the SR store is defined as the gain of CICR [12]. The gain has been used as a parameter to evaluate the effectiveness of CICR under different physiological and pharmacological conditions in cardiac myocytes [13,14]. Surprisingly, the

gain of I_{Ca}-induced Ca^{2+} release in mammalian myocytes is voltage-dependent such that more Ca^{2+} is released per Coulomb of Ca^{2+} influx at voltages negative to zero (high gain) than at positive voltages (0 to +40 mV, lower gain). Irrespective of the mechanisms suggested by different investigators [12], the voltage-dependence of CICR is unique to cardiac EC-coupling, as I_{Ca}-gated Ca^{2+}-release in neurons, for instance, shows no voltage-dependence [39]. To test the voltage-dependence of the gain factor in the human iPS-CMs, we quantified Ca^{2+} release triggered by I_{Ca} as a function of SR Ca^{2+} store at two potentials: −30 mV, where I_{Ca} is marginally activated, and at 0 mV, where I_{Ca} is near its maximal value. Fig. 5G illustrates the quantification of the gain factor at both −30 and 0 mV, in 7 control and 15 mutant myocytes. In a manner similar to adult cardiomyocytes the gain was significantly higher at −30 than at 0 mV, in both control and mutant myocytes (Fig. 5G). The CICR gain though equivalent at 0 mV was significantly larger at −30 mV in mutant compared to control myocytes. Considering the smaller Ca^{2+} content of the SR in mutant myocytes (Fig. 5), this finding suggests a more sensitive Ca^{2+} release mechanism in mutant cells for equivalent I_{Ca} densities (Fig. 2), especially under conditions that would increase the SR load.

The gain factor was calculated using Eq. (1):

$$\text{Gain}=\frac{100\times\Delta F_{I_{\text{Ca}}}}{\Delta F_{I_{\text{Caff}}}\times I_{\text{Ca}}} \quad (1)$$

(where $\Delta F_{I\text{Ca}}$ and $\Delta F_{I\text{caff}}$ are the Ca^{2+}-signals produced, respectively, by activation of I_{Ca} and exposure to caffeine) averaged ~20 in CPVT mutant compared to ~12 in control iPS-CM at −30 mV (Fig. 5G). The higher gain of mutant cells at the threshold of activation of I_{Ca} may contribute to the instability of release mechanism at voltages near resting potentials, especially under Ca^{2+}-overload conditions.

3.3.4. Modulation of SR-stores by isoproterenol—In this set of experiments, we quantified the effect of isoproterenol on the magnitude of caffeine-triggered Ca^{2+} stores and found in control cells a significant enhancement in the magnitude of the store in the presence of isoproterenol (Fig. 6A–E). Interestingly, although the caffeine-triggered Ca^{2+} releases ($\Delta F/F_0$) were significantly enhanced by Isoproterenol (Panel E, upper bar-graphs), the accompanying I_{NCX} were significantly reduced (lower bar-graphs) as may be expected by isoproterenol-induced enhancement of recirculation fraction (R_f) of released Ca^{2+} back into the SR [33]. An attempt to test similar effects of isoproterenol on the size of the caffeine-induced Ca^{2+} transients in mutant cells produced recordings that were difficult to quantify and too variable to yield conclusive results. The variability in the caffeine-releasable fraction of the store in mutant cells treated with isoproterenol appeared to be caused by increased frequency of spontaneously occurring releases in the presence of the hormone that altered significantly the size of the available release-stores, prior to application of caffeine. Fig. 6F shows recordings from mutant cells where such spontaneous Ca^{2+} releases (arrows) are seen interlaced with those activated at 5 s intervals by I_{Ca}. As shown in Fig. 6H, the spontaneous Ca^{2+} releases were abundant only when the Na^+ concentration was increased from 5 to 15 mM, in which case their frequency was larger in mutant (NP0014) than in control cells (WT) and was further increased by isoproterenol. Panel G shows accompanying minor changes in baseline fluorescence (Diastolic Ca^{2+}). These findings are consistent with idea that Ca^{2+} overload of the myocyte is a critical in manifestations of CPVT syndrome.

3.4. Focal Ca^{2+} releases and Ca^{2+} sparks

In intact spontaneously beating cells from control and CPVT-mutant incubated in Fluo-4AM containing solutions, we measured the properties of focal Ca^{2+}-release using two-dimensional confocal imaging with moderate success. Much clearer and more distinct Ca^{2+}-sparks and focal releases were, however, observed when we used a TIRF imaging system (Leica Inc.) with higher spatial resolution (0.1 μm, Fig. 1). Measurements of sparks in control and mutant cells, Fig. 7C, shows a histogram of spark-duration suggesting that control sparks rarely lasted longer than 20 ms, while mutant sparks frequently reached durations of 100 ms or more, consistent with longer mean open time of RyR2s.

Our method of analysis made it possible to determine the location Ca^{2+} sparks in the focal plane with an accuracy of ~0.1 μm (see Section 2 and Fig. 1). Considering that the imaging resolution in the vertical direction, determined by the evanescent field of illumination was also in the order of 0.1 μm, we achieved an overall resolution that revealed distinct sites with properties that were often preserved from one Ca^{2+} release event to the next. Fig. 7D and E suggests that the Ca^{2+} release sites may be classified in different categories. One type of Ca^{2+} release site produced rare and brief Ca^{2+} releases that with imaging speed of 70–100 Hz produced strong, highly localized fluorescence hot-spots in only a single frame (Panel D, Control, #116). These sparks faded and spread in 1–2 frames, but remained centered at the same location. At a second type of Ca^{2+} release site, the events were equally brief, but recurred every few hundred milliseconds (D: Control #56; E: mutant #31). While the latter sites were found in both control and mutant cells, sites with much longer lasting release events were found predominantly in the mutant cells. In some cases the epicenter of the release site remained stationary in several frames (E: Mutant #21 and 103), yet the Ca^{2+} release often appeared to terminate abruptly rather than gradually (Suppl. Fig. 1D). In other cases it leaped from site to site (E: Mutant # 109, Suppl. Fig. 1E). The long-lasting wandering Ca^{2+} release events in the mutant cells may generate inward I_{NCX} that in turn may predispose for EADs and DADs. We consistently found that different Ca^{2+} release sites had distinct properties that were repeatable at different times, but varied from site to site. It may be significant to note that Ca^{2+} release sites in mutant cells had a broad spectrum of Ca^{2+} release times that included the normal brief sparks possibly supporting the idea that the mutation does not by itself cause prolonged wandering Ca^{2+}releases but does so only when other factors come into play.

3.5. Pharmacology of iPS-CM

Pharmacological agents known to activate adrenergic cascade or serve as agonists of Ca^{2+} channel enhance I_{Ca} and potentiate Ca_i-transients in cardiac muscle. Fig. 8 shows the effectiveness of isoproterenol in enhancing I_{Ca} and I_{Ca}-triggered Ca_i-transients in control and CPVT-mutant myocytes. Generally we found that isoproterenol while doubling I_{Ca}, only slightly (~20%) enhanced the Ca^{2+} transients (Fig. 8C and D). Similarly Bay K 8644 also potentiated I_{Ca} strongly, but only moderately enhanced the Ca_i-transients (Suppl. Fig. 3). There appeared to be no significant differential potentiating effects of these agents in control *vs.* the mutant cells.

We also analyzed the extent to which isoproterenol altered the gain of CICR in control and mutant myocytes. Fig. 8 E quantifies the gain factor in control and mutant myocytes at −30 mV where the gain is high and at 0 mV where the gain is lower, as observed in adult ventricular myocytes and confirmed in Fig. 5G in iPS-CMs. Interestingly, isoproterenol appeared to lower the gain at both voltages in control, but not in CPVT-mutant myocytes. Such differential effect of isoproterenol in control and CPVT-mutant myocytes may contribute to higher sensitivity of mutant RyRs to be activated in presence of adrenergic agonists as compared to control cells.

3.6. Effect of dBcAMP on Ca^{2+} signals in intact mutant iPS-CMs

Using TIRF microscopy we found that adrenergic stimulation of mutant iPS-CMs often caused Ca^{2+}-overload. In other cells, that tolerated exposure to 8-Br-cAMP, or di-butryl cAMP for 1–3 min, we generally observed increase in the frequency of spontaneous beating (Fig. 9A *vs.* E), and occasionally periods of increased diastolic Ca^{2+} release activity in the form of bursts of Ca^{2+} sparks and low level Ca^{2+} waves (B *vs.* F). The location of Ca^{2+} sparks were obtained by computerized analysis and are shown as maps superimposed on sample images showing Ca^{2+} sparks (C *vs.* G) or the onset of synchronous activation of Ca^{2+} release (D *vs.* H). These maps suggest that isoproterenol may increase the tendency of focal Ca^{2+} releases to wander or jump (white lines) from one frame to the next. The sites of the mapped Ca^{2+} sparks (white triangles) showed little correlation with the highly reproducible regions of synchronous Ca^{2+} release (D and H) suggesting that the spontaneous diastolic Ca^{2+} sparks may occur at sites that are not fully integrated in I_{Ca}-induced Ca^{2+} release mechanism.

4. Discussion

The major finding of this study is that spontaneously beating cells derived from human skin fibroblast show similar Ca^{2+} signaling properties as those of adult mammalian hearts, *i.e.* they express a robust I_{Ca}-gated CICR signaling pathway modulated by adrenergic and Ca^{2+} channel agonists, Table 1. Nevertheless, there were significant quantitative but not qualitative differences in the density of I_{Ca}, the SR Ca^{2+} load, and the response to adrenergic and Ca^{2+} channel agonists among the control as well as mutant cells, perhaps as a consequence of developmental stage of the myocytes. The most prominent change in the Ca^{2+}signaling profile of p.F2843I RyR2-mutant cells was their consistently smaller caffeine-triggered Ca^{2+} stores and higher CICR gain, resulting most likely from higher frequency of recurrent longer and spatially wandering sparks. Although isoproterenol was equally effective in enhancing I_{Ca}, Ca_i-transients, and caffeine-triggered Ca^{2+}-stores in control and mutant cells (Figs. 6 and 8), it differentially increased the diastolic Ca^{2+} levels, and the frequency of spontaneous Ca^{2+} releases in mutant cells (Fig. 6F). Given the altered Ca^{2+} signaling profile of CPVT-mutant cells, it is likely that such cells when exposed to conditions that increase the SR Ca^{2+} load, such as adrenergic stimulation, higher beating frequency, and increased cytosolic Na^{+} load, would render the mutant myocytes in intact heart more susceptible to triggering of DADs or EADs, and arrhythmogenesis. In this study we have attempted to perform a detailed investigation of Ca^{2+} signaling parameters at room temperature (22–24 °C) in iPS-CMs derived from a control subject and from a single patient with the novel F2843I mutation of the cardiac ryanodine receptor. Thus it remains to be examined how the cells may perform at physiological temperatures and although CPVT is a Mendelian disease, there may be modifying factors that impose on the role of RYR2 in EC-coupling and therefore cause variability from one patient to another carrying the same mutation. It should be also noted that working with single cells did not allow direct examination of arrhythmogenic characteristics that depend on electrical communication between cells.

4.1. Ca^{2+} stores and their regulation: control vs. mutant

In cardiac-type EC-coupling there are three critical elements that contribute to the effectiveness of CICR: the density of I_{Ca}, the activation-state of RyRs, and magnitude of the Ca^{2+} stores. This has been amply demonstrated by many investigators and is confirmed here by the bell-shaped voltage-dependence of Ca_i-transients reflecting the voltage-dependence of I_{Ca} (Fig. 3). This characteristic appears to be fully intact in CPVT-mutant myocytes. Interestingly, the fractional Ca^{2+} release seems to be higher in mutant cells, but the effect was not statistically significant (Fig. 4C).

A novel and consistent finding of our studies, also reported for P2328S iPSC-CMs [40] and in R4496C knock-in mice model [27], was that the caffeine-triggered Ca^{2+}-stores were significantly smaller in mutant cells (Fig. 5E). The lower Ca^{2+} store content is likely to be caused by enhanced mean open time of RyRs (leakiness) reported in almost every animal model of CPVT, irrespective of the alternative mechanisms proposed. It is clear that a lower Ca^{2+}-content of SR in hearts with hyperactive RyR2s would serve as a protective compensatory mechanism to reduce irregularities in rate and rhythm in whole animal models. Our finding of similar decreases in the SR Ca^{2+}-content in human cellular model of CPVT, suggests that such compensatory decreases are likely to result from the molecular cross-talk between the cellular Ca^{2+}-signaling proteins.

The Ca^{2+}-content of the SR was measured either by using Fluo-4 Ca^{2+}-sensing dye or by the integral of NCX current generated in response to rise of intracellular Ca^{2+} by caffeine. The total charge carried by I_{NCX} (Fig. 5F) provides a more accurate estimate of Ca^{2+} extruded from the cytosol following application of caffeine, as this measurement is free of complications resulting from dye-saturation or quantification of Ca^{2+} using a non-ratio-metric fluorescent dyes. Fig. 5F and G confirms the findings of Fig. 5E that the mutant Ca^{2+} stores are significantly smaller than those of control myocytes, but in addition shows that cellular conditions that increase the cytosolic load of Ca^{2+}, for instance, higher intracel-lular Na^{+}, can strongly enhance the Ca^{2+} content of the stores in mutant cells. A similar loading of Ca^{2+} store seems also to occur on exposure of cells to isoproterenol (Fig. 6E). In the latter case, even though the caffeine-triggered Ca^{2+}-release (Fluo-4 signal) is strongly enhanced by isoproterenol, the accompanying I_{NCX} is suppressed significantly as maybe predicted from the PKA-induced enhancement of SERCA2a/PLB activity and the increased re-uptake of Ca^{2+} into the SR, *i.e.* the enhancement of recirculating fraction (R_f) of Ca^{2+} [33].

4.2. Gain of CICR

In a purely CICR-gated signaling system, only the numbers of coulombs of Ca^{2+} that enter the cell and interact with RyRs determine the magnitude of released Ca^{2+}. Such a strictly Ca^{2+}-, but not voltage-dependent property of CICR has been observed in neurons [39]. In cardiac myocytes, however, CICR gain shows significant voltage-dependence, such that the gain increases exponentially at voltages negative to 0 mV [41]. This voltage-dependence remains controversial [12] as it may depend not only on the unitary currents and open probability of the Ca^{2+} channels [42], but also on their mean open time and the structure of the dyadic junctions which in turn may be altered under pathological conditions with respect to geometry and complements of Ca^{2+} channels and RyRs. Interestingly, in atrial myocytes only the surface, but not the centrally located RyRs appear to show the cardiac phenotypic voltage-dependent gain. Woo et al. [43] by introducing various fragments of carboxyl-tail of Ca^{2+}-channel into atrial myocytes probed for possible interactions between specific domains of carboxyl tail and RyR2 in mediating the voltage-dependent gain of CICR. In support of direct interaction of DHPR with RyRs it was found that only the CaMKII/CaM binding fragment (LA) of the carboxylic tail of the DHPR [44] rendered voltage-dependence to the centrally located “naked” RyRs when the fragment was introduced into the atrial myocyte [43]. Irrespective of the underlying mechanism for the voltage-dependence of CICR, it is clear that hiPSC-CMs show not only voltage-dependent gain of CICR, but also comparatively enhanced gain at negative potentials in mutant cells (Fig. 5G), making the CPVT-mutant myocyte Ca^{2+}-signaling mechanisms poised for release.

4.3. CPVT Ca^{2+}-signaling models: of mice and men

The CPVT cellular model presented here was made possible by the finding that the p.F2483I mutation could be expressed in the iPSC-derived cardiomyocytes from the fibroblasts of a patient afflicted with CPVT [9], making it possible to study the pathophysiology of human

disease in the laboratory setting. Considering the large number (>80) of point mutations in RyRs that bring about CPVT, it is difficult to generalize that this point mutation would have the same Ca^{2+}-signaling profile as those reported for other point mutations either in transgenic mice (R2474S [45]; S2246L [28]; P2328 in [26]; and R4496C [27,46]) or in iPS-CM (M4109R [47]; S406L [48]; and P2328S [40] 2012). It is more likely that there will be subtle differences in Ca^{2+}-signaling profiles of the various models, because the proposed mechanisms responsible for enhancement of diastolic Ca^{2+} release in CPVT1 vary from: (1) altered sensitivity of mutant RyR2, (2) activation by luminal Ca^{2+}, (3) decreased FKBP12.6 binding to mutant RYR2 and (4) to abnormal local intermolecular RYR2 domain interactions. Our findings, summarized in Table 1, suggest that p.F2483I mutation produces unitary Ca^{2+} release events that are longer in duration, more wandering and recurrent in nature, and therefore are likely to lead to activation of Ca^{2+}-waves and generation of EADs and DADs. Although in some mutant cells we observed higher frequencies of spark occurrence, we believe that such measurements in intact cells are less reliable as the frequency of sparks, even in control cells, may vary greatly depending on physiological state of the myocyte. Cells that showed higher spark frequencies are likely to be more Ca^{2+}-overloaded. Interestingly, we found consistently that exposure of myocytes to isoproterenol increased the proclivity of sparks to migrate/wander and generate diastolic rises of Ca^{2+} as the frequency of spontaneous beating increased (Figs. 6 and 9). In 15 mM Na^+ dialyzed mutant cells, held at −40 mVs, we often found higher frequencies of spontaneous releases of Ca^{2+} (accompanied by activation of equivalent I_{NCX}) than in control cells, or mutant cells dialyzed with 5 mM Na^+, consistent with the idea that Ca^{2+}-overloading conditions increase the proclivity to aberrant Ca^{2+} releases in mutant Cells.

The consistent decrease in the Ca^{2+}-content of the SR (Fig. 5) in the mutant myocytes observed in our study and in recently reported CPVT-iPS-CM carrying P2328S mutation in RYR2 [40] might be expected considering the generally agreed upon finding of increased mean open time of mutant RyRs, irrespective of underlying mechanisms. Nevertheless, in mice knock-in CPVT model with S2246L mutation in RYR2 [28] Ca^{2+}-content of the SR appears not to have changed significantly even though spark frequency was markedly increased. On the other hand, the Gomez group [27] found that R4496C mutation decreased the Ca^{2+} content of the SR, while increasing the spark frequency, consistent with our findings of smaller Ca^{2+}-content of the SR. It is of course possible that the transgenic mice models with heart rates exceeding 500 beats/min do not adequately represent the pathology of human CPVT where the heart is working at ~60 beats/min. We posit that the lower Ca^{2+}-content of the SR in human CPVT may serve as a compensatory protective mechanism to dampen the higher gain of CICR, and the longer and more recurrent spark activity of the CPVT myocytes. The findings that both higher cellular Na^+ load and exposure to isoproterenol strongly increase the SR Ca^{2+} load in our model leads us to suggest that such conditions would overcome the protective compensatory decreases in the SR Ca^{2+}content, that leads to aberrant Ca^{2+}-release and arrhythmias.

Supplementary Material

Refer to Web version on PubMed Central for supplementary material.

Acknowledgments

Funding

Supported by: NIH, RO1-HL16152, RO1-HL107600 to M.M.; Federal Ministry for Education and Science (BMBF, grant number 01GN0824) to T.Š. and J.H., Imhof Stiftung to T. Š. and Köln Fortune Program to T. Š.

A murine visceral endoderm-like cell line was generously provided by C. Mummery, Leiden University Medical Center, The Netherlands.

References

1. Takahashi K, Tanabe K, Ohnuki M, Narita M, Ichisaka T, Tomoda K, Yamanaka S. Induction of pluripotent stem cells from adult human fibroblasts by defined factors. Cell. 2007; 131:861–872. [PubMed: 18035408]
2. Gupta MK, Illich DJ, Gaarz A, Matzkies M, Nguemo F, Pfannkuche K, Liang H, Classen S, Reppel M, Schultze JL, Hescheler J, Saric T. Global transcriptional profiles of beating clusters derived from human induced pluripotent stem cells and embryonic stem cells are highly similar. BMC Developmental Biology. 2010; 10:98. [PubMed: 20843318]
3. Zhang J, Wilson GF, Soerens AG, Koonce CH, Yu J, Palecek SP, Thomson JA, Kamp TJ. Functional cardiomyocytes derived from human induced pluripotent stem cells. Circulation Research. 2009; 104:e30–e41. [PubMed: 19213953]
4. Hoekstra M, Mummery CL, Wilde AA, Bezzina CR, Verkerk AO. Induced pluripotent stem cell derived cardiomyocytes as models for cardiac arrhythmias. Frontiers in Physiology. 2012; 3:346. [PubMed: 23015789]
5. Moretti A, Bellin M, Welling A, Jung CB, Lam JT, Bott-Flugel L, Dorn T, Goedel A, Hohnke C, Hofmann F, Seyfarth M, Sinnecker D, Schomig A, Laugwitz KL. Patient-specific induced pluripotent stem-cell models for long-QT syndrome. New England Journal of Medicine. 2010; 363:1397–1409. [PubMed: 20660394]
6. Itzhaki I, Maizels L, Huber I, Zwi-Dantsis L, Caspi O, Winterstern A, Feldman O, Gepstein A, Arbel G, Hammerman H, Boulos M, Gepstein L. Modelling the long QT syndrome with induced pluripotent stem cells. Nature. 2011; 471:225–229. [PubMed: 21240260]
7. Matsa E, Rajamohan D, Dick E, Young L, Mellor I, Staniforth A, Denning C. Drug evaluation in cardiomyocytes derived from human induced pluripotent stem cells carrying a long QT syndrome type 2 mutation. European Heart Journal. 2011; 32:952–962. [PubMed: 21367833]
8. Malan D, Friedrichs S, Fleischmann BK, Sasse P. Cardiomyocytes obtained from induced pluripotent stem cells with long-QT syndrome 3 recapitulate typical disease-specific features in vitro. Circulation Research. 2011; 109:841–847. [PubMed: 21799153]
9. Fatima A, Xu G, Shao K, Papadopoulos S, Lehmann M, Arnaiz-Cot JJ, Rosa AO, Nguemo F, Matzkies M, Dittmann S, Stone SL, Linke M, Zechner U, Beyer V, Hennies HC, Rosenkranz S, Klauke B, Parwani AS, Haverkamp W, Pfitzer G, Farr M, Cleemann L, Morad M, Milting H, Hescheler J, Saric T. In vitro modeling of ryanodine receptor 2 dysfunction using human induced pluripotent stem cells. Cellular Physiology and Biochemistry. 2011; 28:579–592. [PubMed: 22178870]
10. Lahti AL, Kujala VJ, Chapman H, Koivisto AP, Pekkanen-Mattila M, Kerkela E, Hyttinen J, Kontula K, Swan H, Conklin BR, Yamanaka S, Silvennoinen O, Aalto-Setala K. Model for long QT syndrome type 2 using human iPS cells demonstrates arrhythmogenic characteristics in cell culture. Disease Models and Mechanisms. 2012; 5:220–230. [PubMed: 22052944]
11. Davis RP, Casini S, van den Berg CW, Hoekstra M, Remme CA, Dambrot C, Salvatori D, Oostwaard DW, Wilde AA, Bezzina CR, Verkerk AO, Freund C, Mummery CL. Cardiomyocytes derived from pluripotent stem cells recapitulate electrophysiological characteristics of an overlap syndrome of cardiac sodium channel disease. Circulation. 2012; 125:3079–3091. [PubMed: 22647976]
12. Wier WG. Gain and cardiac E–C coupling: revisited and revised. Circulation Research. 2007; 101:533–535. [PubMed: 17872469]
13. Adachi-Akahane S, Cleemann L, Morad M. Cross-signaling between L-type Ca^{2+} channels and ryanodine receptors in rat ventricular myocytes. Journal of General Physiology. 1996; 108:435–454. [PubMed: 8923268]
14. Bers DM, Guo T. Calcium signaling in cardiac ventricular myocytes. Annals of the New York Academy of Sciences. 2005; 1047:86–98. [PubMed: 16093487]
15. Dolnikov K, Shilkrut M, Zeevi-Levin N, Gerecht-Nir S, Amit M, Danon A, Itskovitz-Eldor J, Binah O. Functional properties of human embryonic stem cell-derived cardiomyocytes:

intracellular Ca^{2+} handling and the role of sarcoplasmic reticulum in the contraction. Stem Cells. 2006; 24:236–245. [PubMed: 16322641]

16. Liu J, Fu JD, Siu CW, Li RA. Functional sarcoplasmic reticulum for calcium handling of human embryonic stem cell-derived cardiomyocytes: insights for driven maturation. Stem Cells. 2007; 25:3038–3044. [PubMed: 17872499]
17. Sedan O, Dolnikov K, Zeevi-Levin N, Leibovich N, Amit M, Itskovitz-Eldor J, Binah O. 1,4,5-Inositol trisphosphate-operated intracellular Ca(2+) stores and angiotensin-II/endothelin-1 signaling pathway are functional in human embryonic stem cell-derived cardiomyocytes. Stem Cells. 2008; 26:3130–3138. [PubMed: 18818435]
18. Itzhaki I, Rapoport S, Huber I, Mizrahi I, Zwi-Dantsis L, Arbel G, Schiller J, Gepstein L. Calcium handling in human induced pluripotent stem cell derived cardiomyocytes. PLoS ONE. 2011; 6:e18037. [PubMed: 21483779]
19. Zhu WZ, Santana LF, Laflamme MA. Local control of excitation–contraction coupling in human embryonic stem cell-derived cardiomyocytes. PLoS ONE. 2009; 4:e5407. [PubMed: 19404384]
20. Ginsburg KS, Bers DM. Modulation of excitation–contraction coupling by isoproterenol in cardiomyocytes with controlled SR Ca^{2+} load and Ca^{2+} current trigger. Journal of Physiology. 2004; 556:463–480. [PubMed: 14724205]
21. He LP, Cleemann L, Soldatov NM, Morad M. Molecular determinants of cAMP-mediated regulation of the Na^{+}–Ca^{2+} exchanger expressed in human cell lines. Journal of Physiology. 2003; 548:677–689. [PubMed: 12626672]
22. Marks AR, Priori S, Memmi M, Kontula K, Laitinen PJ. Involvement of the cardiac ryanodine receptor/calcium release channel in catecholaminergic polymorphic ventricular tachycardia. Journal of Cellular Physiology. 2002; 190:1–6. [PubMed: 11807805]
23. Lehnart SE, Wehrens XH, Marks AR. Calstabin deficiency, ryanodine receptors, and sudden cardiac death. Biochemical and Biophysical Research Communications. 2004; 322:1267–1279. [PubMed: 15336974]
24. Jiang D, Wang R, Xiao B, Kong H, Hunt DJ, Choi P, Zhang L, Chen SR. Enhanced store overload-induced Ca^{2+} release and channel sensitivity to luminal Ca^{2+} activation are common defects of RyR2 mutations linked to ventricular tachycardia and sudden death. Circulation Research. 2005; 97:1173–1181. [PubMed: 16239587]
25. Priori SG, Chen SR. Inherited dysfunction of sarcoplasmic reticulum Ca^{2+} handling and arrhythmogenesis. Circulation Research. 2011; 108:871–883. [PubMed: 21454795]
26. Goddard CA, Ghais NS, Zhang Y, Williams AJ, Colledge WH, Grace AA, Huang CL. Physiological consequences of the P2328S mutation in the ryanodine receptor (RyR2) gene in genetically modified murine hearts. Acta Physiologica (Oxford). 2008; 194:123–140.
27. Fernandez-Velasco M, Rueda A, Rizzi N, Benitah JP, Colombi B, Napolitano C, Priori SG, Richard S, Gomez AM. Increased Ca^{2+} sensitivity of the ryanodine receptor mutant RyR2R4496C underlies catecholaminergic polymorphic ventricular tachycardia. Circulation Research. 2009; 104:201–209. 12p following 209. [PubMed: 19096022]
28. Suetomi T, Yano M, Uchinoumi H, Fukuda M, Hino A, Ono M, Xu X, Tateishi H, Okuda S, Doi M, Kobayashi S, Ikeda Y, Yamamoto T, Ikemoto N, Matsuzaki M. Mutation-linked defective interdomain interactions within ryanodine receptor cause aberrant Ca(2)(+)release leading to catecholaminergic polymorphic ventricular tachycardia. Circulation. 2011; 124:682–694. [PubMed: 21768539]
29. Cerrone M, Colombi B, Santoro M, di Barletta MR, Scelsi M, Villani L, Napolitano C, Priori SG. Bidirectional ventricular tachycardia and fibrillation elicited in a knock-in mouse model carrier of a mutation in the cardiac ryanodine receptor. Circulation Research. 2005; 96:e77–e82. [PubMed: 15890976]
30. Woo SH, Cleemann L, Morad M. Diversity of atrial local Ca^{2+} signalling: evidence from 2-D confocal imaging in Ca^{2+}-buffered rat atrial myocytes. Journal of Physiology. 2005; 567:905–921. [PubMed: 16020459]
31. Cleemann L, Wang W, Morad M. Two-dimensional confocal images of organization, density, and gating of focal Ca^{2+} release sites in rat cardiac myocytes. Proceedings of the National Academy of Sciences of the United States of America. 1998; 95:10984–10989. [PubMed: 9724816]

32. Tufan H, Zhang XH, Haghshenas N, Sussman MA, Cleemann L, Morad M. Cardiac progenitor cells engineered with Pim-1 (CPCeP) develop cardiac phenotypic electrophysiological properties as they are co-cultured with neonatal myocytes. Journal of Molecular and Cellular Cardiology. 2012; 53:695–706. [PubMed: 23010478]
33. Morad M, Goldman Y. Excitation–contraction coupling of heart muscle: membrane control of development of tension. Progress in Biophysics and Molecular Biology. 1973; 27:257–313.
34. Cleemann L, Morad M. Role of Ca^{2+} channel in cardiac excitation–contraction coupling in the rat: evidence from Ca^{2+} transients and contraction. Journal of Physiology. 1991; 432:283–312. [PubMed: 1653321]
35. Bers DM. Calcium cycling and signaling in cardiac myocytes. Annual Review of Physiology. 2008; 70:23–49.
36. Woo SH, Cleemann L, Morad M. Spatiotemporal characteristics of junctional and nonjunctional focal Ca^{2+} release in rat atrial myocytes. Circulation Research. 2003; 92:e1–e11. [PubMed: 12522129]
37. Belmonte S, Morad M. 'Pressure-flow'-triggered intracellular Ca^{2+} transients in rat cardiac myocytes: possible mechanisms and role of mitochondria. Journal of Physiology. 2008; 586:1379–1397. [PubMed: 18187469]
38. Bassani JW, Yuan W, Bers DM. Fractional SR Ca release is regulated by trigger Ca and SR Ca content in cardiac myocytes. American Journal of Physiology. 1995; 268:C1313–C1319. [PubMed: 7762626]
39. Solovyova N, Veselovsky N, Toescu EC, Verkhratsky A. Ca(2+) dynamics in the lumen of the endoplasmic reticulum in sensory neurons: direct visualization of Ca(2+)-induced Ca(2+) release triggered by physiological Ca(2+) entry. EMBO Journal. 2002; 21:622–630. [PubMed: 11847110]
40. Kujala K, Paavola J, Lahti A, Larsson K, Pekkanen-Mattila M, Viitasalo M, Lahtinen AM, Toivonen L, Kontula K, Swan H, Laine M, Silvennoinen O, Aalto-Setala K. Cell model of catecholaminergic polymorphic ventricular tachycardia reveals early and delayed afterdepolarizations. PLoS ONE. 2012; 7:e44660. [PubMed: 22962621]
41. Adachi-Akahane S, Cleemann L, Morad M. BAY K 8644 modifies Ca^{2+} cross signaling between DHP and ryanodine receptors in rat ventricular myocytes. American Journal of Physiology. 1999; 276:H1178–H1189. [PubMed: 10199841]
42. Altamirano J, Bers DM. Voltage dependence of cardiac excitation–contraction coupling: unitary Ca^{2+} current amplitude and open channel probability. Circulation Research. 2007; 101:590–597. [PubMed: 17641229]
43. Woo SH, Soldatov NM, Morad M. Modulation of Ca^{2+} signalling in rat atrial myocytes: possible role of the alpha1C carboxyl terminal. Journal of Physiology. 2003; 552:437–447. [PubMed: 14561827]
44. Soldatov NM, Zuhlke RD, Bouron A, Reuter H. Molecular structures involved in L-type calcium channel inactivation. Role of the carboxyl-terminal region encoded by exons 40–42 in alpha1C subunit in the kinetics and Ca^{2+} dependence of inactivation. Biological Chemistry. 1997; 272:3560–3566.
45. Lehnart SE, Mongillo M, Bellinger A, Lindegger N, Chen BX, Hsueh W, Reiken S, Wronska A, Drew LJ, Ward CW, Lederer WJ, Kass RS, Morley G, Marks AR. Leaky Ca^{2+} release channel/ryanodine receptor 2 causes seizures and sudden cardiac death in mice. Journal of Clinical Investigation. 2008; 118:2230–2245. [PubMed: 18483626]
46. Liu N, Colombi B, Memmi M, Zissimopoulos S, Rizzi N, Negri S, Imbriani M, Napolitano C, Lai FA, Priori SG. Arrhythmogenesis in catecholaminergic polymorphic ventricular tachycardia: insights from a RyR2 R4496C knock-in mouse model. Circulation Research. 2006; 99:292–298. [PubMed: 16825580]
47. Itzhaki I, Maizels L, Huber I, Gepstein A, Arbel G, Caspi O, Miller L, Belhassen B, Nof E, Glikson M, Gepstein L. Modeling of catecholaminergic polymorphic ventricular tachycardia with patient-specific human-induced pluripotent stem cells. Journal of the American College of Cardiology. 2012; 60:990–1000. [PubMed: 22749309]
48. Jung CB, Moretti A, Mederos y Schnitzler M, Iop L, Storch U, Bellin M, Dorn T, Ruppenthal S, Pfeiffer S, Goedel A, Dirschinger RJ, Seyfarth M, Lam JT, Sinnecker D, Gudermann T, Lipp P,

Laugwitz KL. Dantrolene rescues arrhythmogenic RYR2 defect in a patient-specific stem cell model of catecholaminergic polymorphic ventricular tachycardia. EMBO Molecular Medicine. 2012; 4:180–191. [PubMed: 22174035]

Appendix A. Supplementary data

Supplementary data associated with this article can be found, in the online version, at doi: 10.1016/j.ceca.2013.04.004.

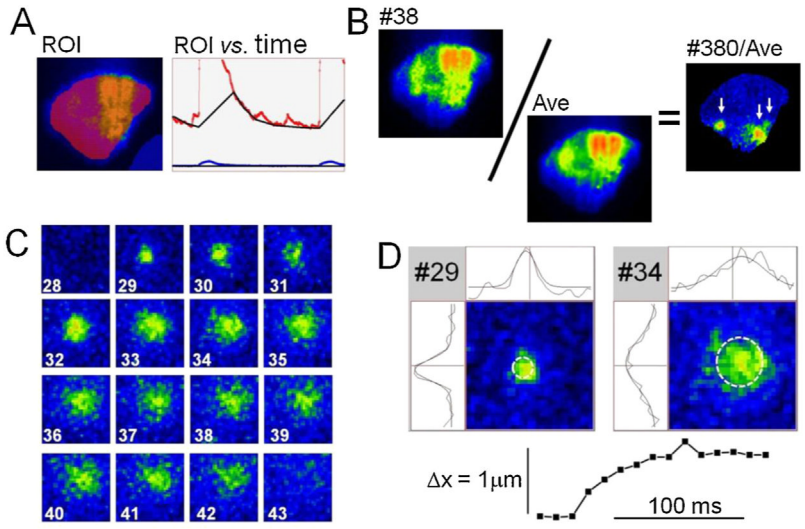

Fig. 1.

Automated analysis of Ca^{2+} sparks based on TIRF-imaging. (A) Equalization of the diastolic fluorescence intensity. The image (ROI) shows a single frame with superimposed regions of interest that were marked in a semi-transparent manner in red (cell) and blue (surroundings). The fluorescence intensities in these regions were plotted *versus* time (red and blue curves), and were approximated throughout the diastolic intervals by a black curve and a line that together determined a scale factor that varied with time and was used to compensate for the slow decline in fluorescence that often occurred in the intervals between beats. (B) Ratiometric images. The distribution of fluorescence intensity in each frame (*e.g.* #38) was divided by an average fluorescence intensity calculated based on multiple selected fluorescence images without noticeable Ca^{2+}-release activity. (C) A sequence of partial ratiometric images where the development and decay of local Ca^{2+} release is shown in bright colors on a dark blue mottled background representing the resting Ca^{2+} activity. (D) Determination of unitary properties of Ca^{2+} release based on a Gaussian approximation. The two sample images (#29 and #34) are shown with superimposed white circles that mark the location and standard deviations of Gaussian approximations. The curves above and to the left of the images show how well horizontal and vertical mid sections through the images were approximated by Gaussian curves. The graph at the bottom of Panel D quantifies the horizontal shift in center of the Gaussian approximations as seen also in the curves above the sample images. The shown partial frames correspond to 30 × 30 pixels or 9.4 μm × 9.4 μm.

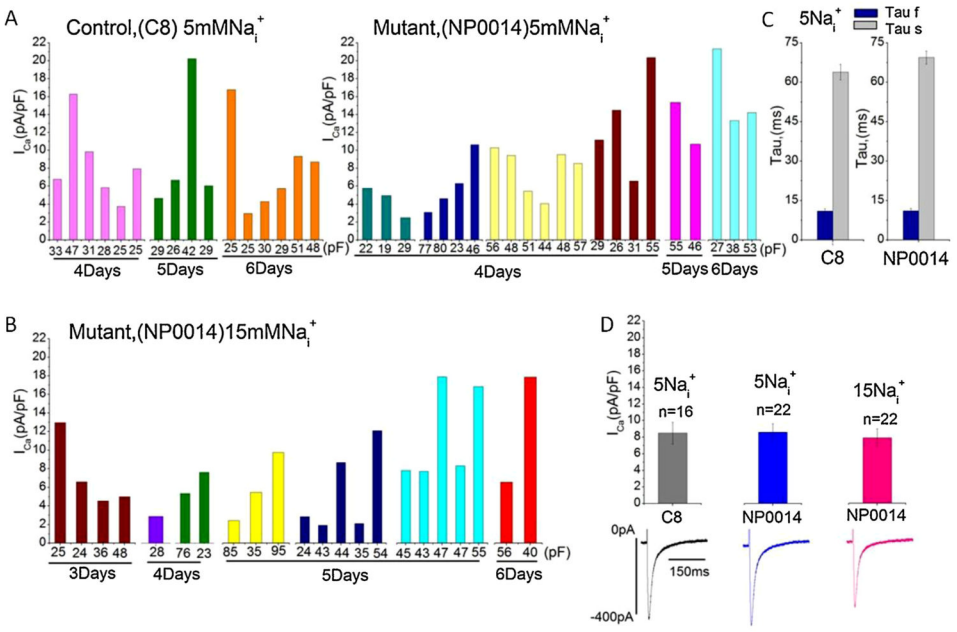

Fig. 2.

Distribution of calcium currents (I_{Ca}) density and average time constant (tau) in control (IMR-C8) and mutant (NP0014-C1) iPS-CM. Cells were cultured for 3–6 days. I_{Ca} was recorded from a holding potential −40 mV with step depolarization to 0 mV. The number at the bottom of each bar indicates the capacitance of individual cells. (Panels A and B) Distribution of I_{Ca} density in control and mutant iPS-CM recorded with $[Na^+]_i$ at 5 or 15 mM Na^+_i. C: Average fast (tau *f*) and slow (tau *s*) time constants of inactivation of I_{Ca} in control and mutant iPS-CM recorded with 5 mM Na^+ in the pipette solution. (D) Average I_{Ca} density of control and mutant iPS-CM and representative I_{Ca} traces from each group. The average membrane capacitance values were: Panel A, IMR-C8, 32.7 ± 2.3 pF, NP0014, 43.6 ± 3.7 pF, and Panel B, NP0014, 45.8 ± 4.2 pF.

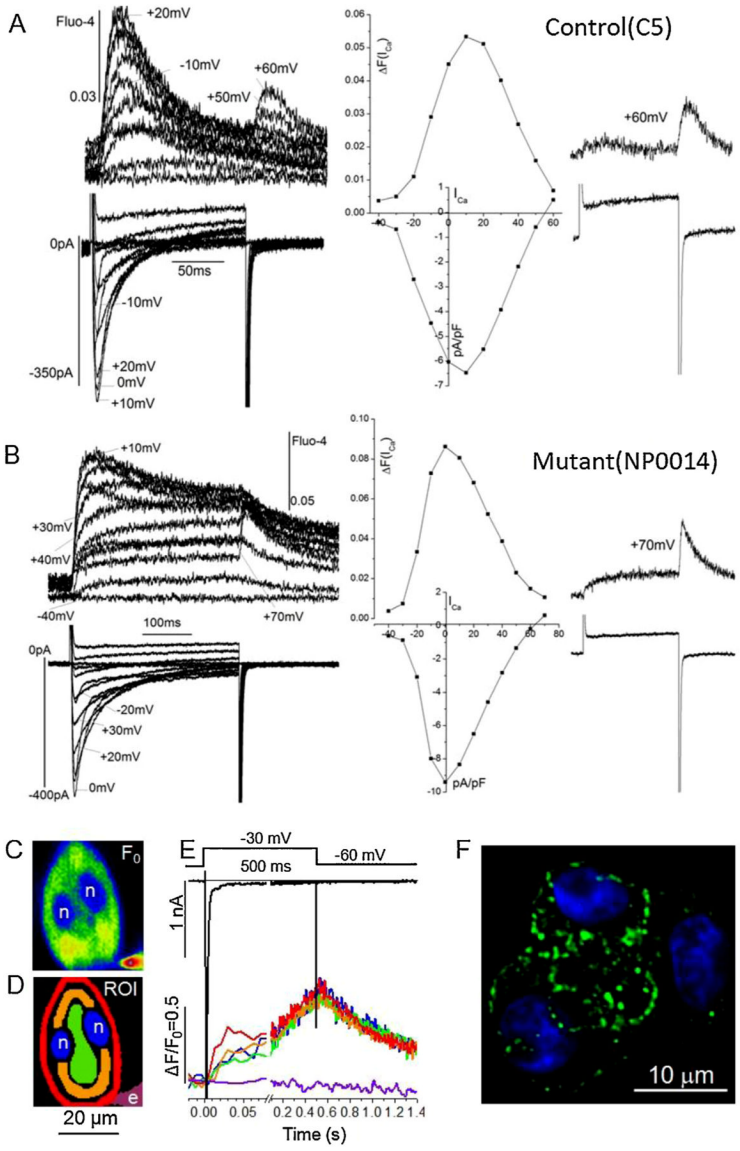

Fig. 3.

Voltage-dependence and subcellular distribution of I_{Ca} -activated Ca^{2+} -transients. Representative current–voltage (I–V) relations normalized relative to the membrane capacitance and the corresponding fluorescence (Fluo-4) Ca^{2+} signal recorded from control (C5, Panel A) and mutant (NP0014, Panel B) iPS-CM. Currents were recorded with a 250 ms step depolarizations from holding potential of −50 mV in 10 mV steps to +60 mV. The middle panel shows the I–V curves for I_{Ca} and the corresponding Ca^{2+} Fluo-4 signal. The internal solution contained 5 mM Na^+, and was Ca^{2+}-buffered with 0.1 mM Fluo-4, 0.2 mM EGTA, and 0.1 mM Ca^{2+}. The right panel shows the I_{Ca} and fluorescence traces at +60 or +70 mV activating rises in Ca^{2+} on repolarization. (C) Confocal image of baseline fluorescence (Fluo-4, F_0). (D) Color-coded regions of interest (ROI) corresponding to nuclei (*n*), patch electrode (*e*) and cytoplasmic regions with increasing distances from the cell membrane (red, orange, green). (E) Differences in the time course of the normalized Ca^{2+}-dependent fluorescence ($\Delta F/F_0$). The color coded traces corresponds to the ROI in Panel D. The 2-D confocal fluorescence images were recorded at 120 Hz using a focal plane

intersecting the nuclei. The initial response is shown on an expanded time scale. The voltage-clamp pulse (from −60 to −30 mV) and the resulting (Na^+ and Ca^{2+}) membrane currents are shown at the top. (F) Confocal image of immunofluorescence labeled RyR2 (green) in a small cluster of control iPS-CM with DAPI-labeled nuclei (blue).

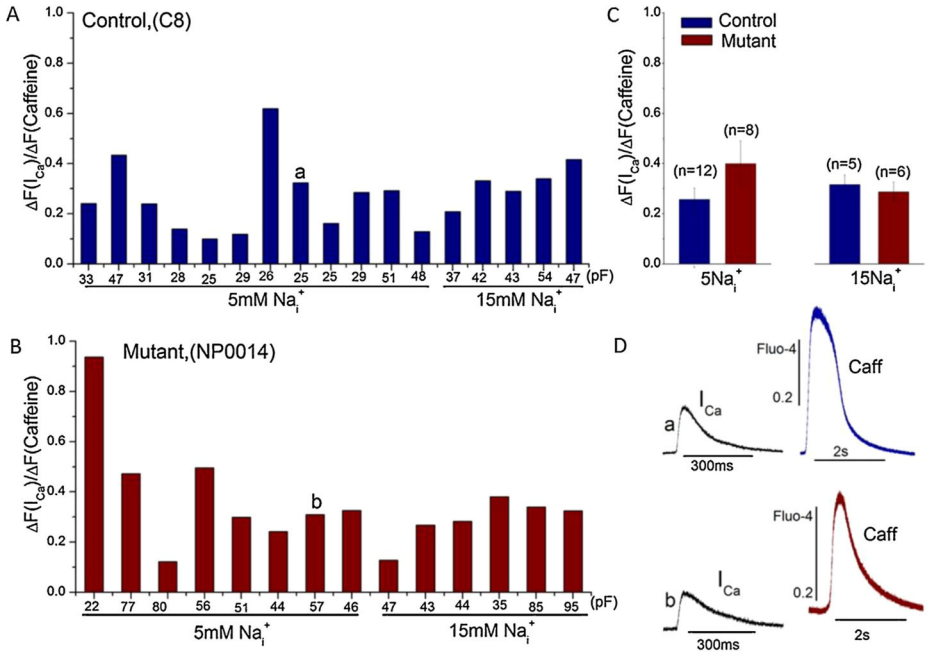

Fig. 4.

Fractional Ca^{2+} release in control and mutant iPS-CM. Fractional release was calculated by dividing the I_{Ca} -triggered Ca_i -transient by that generated by application of caffeine ($\Delta F_{(I_{Ca})}/\Delta F_{(Caff)}$). Cells were voltage-clamped from −50 to 0 mV or were held at −50 mV while subjecting them to 0.5 s long 3 mM caffeine pulses. (A and B) Distribution of the value of efficiency in control (A) and mutant iPS-CM (B). The numbers at the bottom of each bar indicate the membrane capacitance of each cell. (C) Average fractional Ca^{2+} release with 5 and 15 mM Na^+ in the pipette solution. (D) Representative Ca^{2+} signals triggered by I_{Ca} or caffeine in control (a) and mutant (b) iPS-CM.

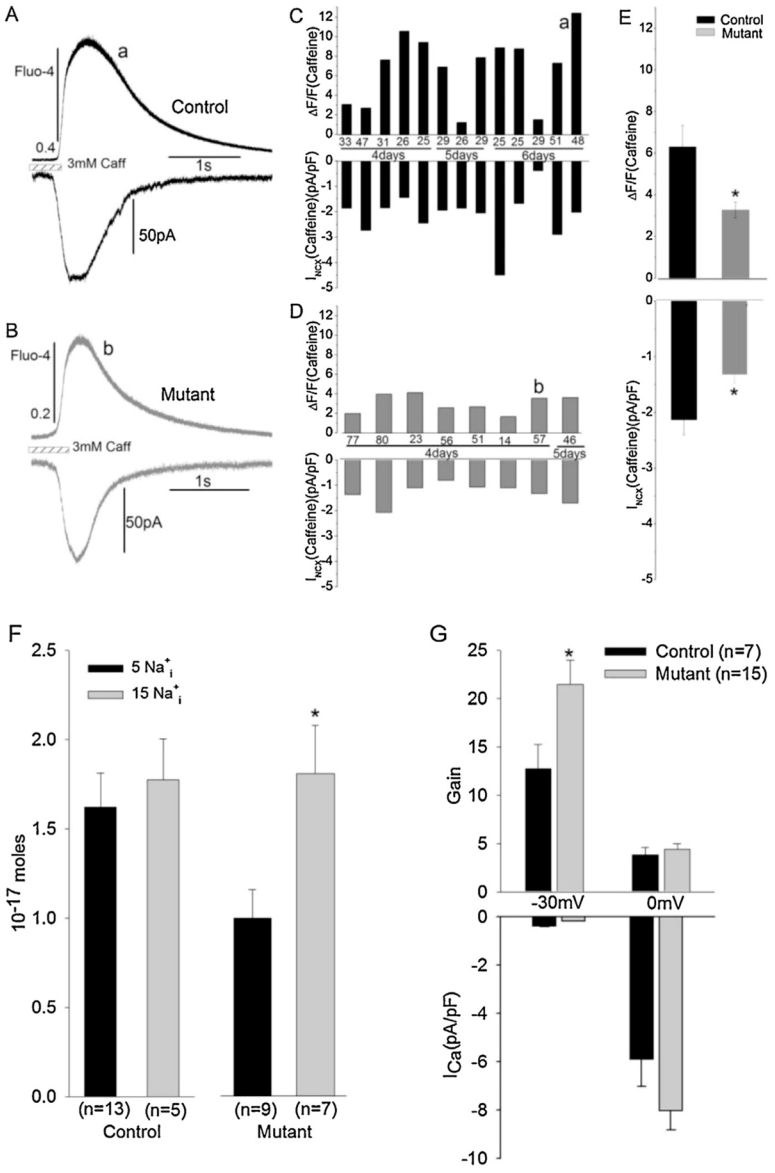

Fig. 5.

Caffeine-releasable Ca^{2+} stores. (A–E) Simultaneous measurements of caffeine-induced I_{NCX} current and Ca^{2+} -dependent fluorescence ($\Delta F/F_0$) in control (IMR-C8) and mutant (NP0014) iPS-CM dialyzed with 5 mM Na^+ and superfused with standard Tyrode's solution. Cells were voltage-clamped to −50 mV and exposed rapidly to 3 mM caffeine for 500 ms. (A and B) Representative caffeine-induced NXC currents and corresponding fluorescence Ca^{2+} signal from control (a) and mutant iPS-CM (b). (C and D) Distribution of I_{NCX} values in control and mutant iPS-CM. (E) Average values of caffeine-activated Ca^{2+} signals (top) I_{NCX} currents (bottom) in each group. Stars indicate significance levels (*$p < 0.05$, **$p < 0.01$). (F and G) Effect of intracellular Na^+ on the amount of Ca^{2+} released from SR in response to application of caffeine. Average values of Ca^{2+} release from SR calculated from the integral of the caffeine-induced I_{NCX} in control and mutant iPS-CM with 5 or 15 mM Na^+ in the internal solution. (G) Average valves of gain factor and I_{Ca} density at −30 and 0 mV. The gain factor is plotted in units corresponding to the fraction in % of the caffeine-induced Ca^{2+} release that is release by a Ca^{2+} current with a density of 1 pA/pF.

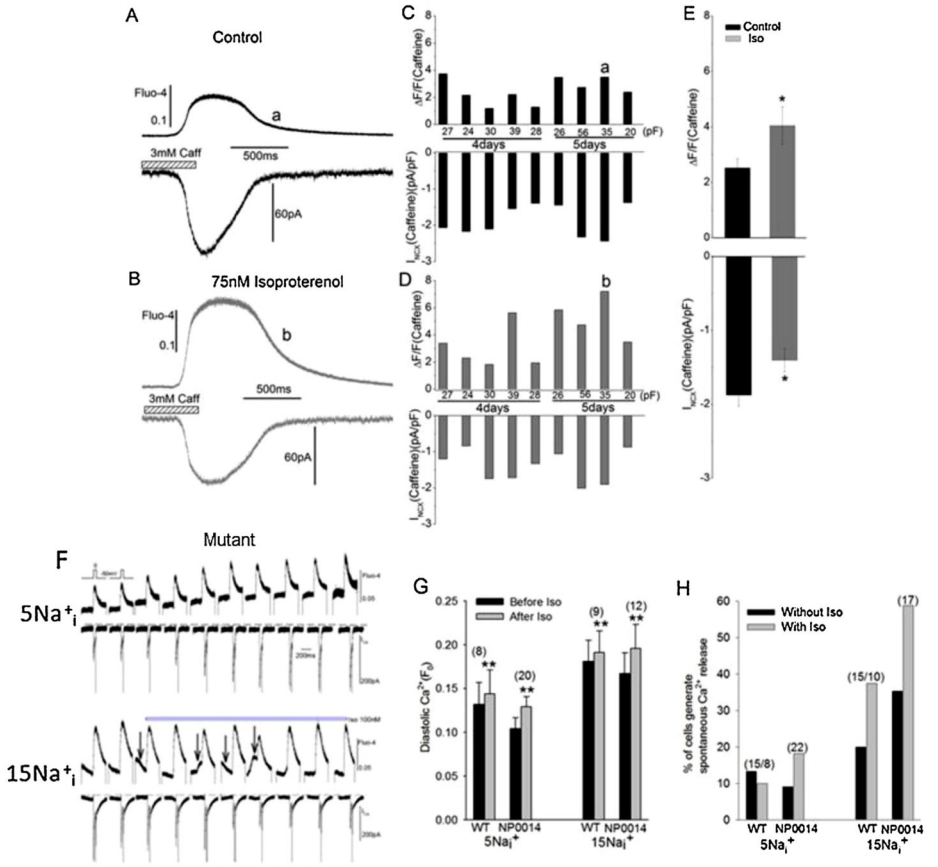

Fig. 6.

Effects of isoproterenol. (A–E) Caffeine-induced I_{NCX} current in control iPS-CM (IMR-C5) recorded with 5 mM Na^+_i before and after exposure to isoproterenol. (A and B) Representative I_{NCX} currents and corresponding fluorescence Ca^{2+} signal before (A) and after (B) exposure to 75 nM isoproterenol. (C and D) Distribution of Ca_i-transients ($\Delta F/F_0$) and I_{NCX} values before (C) and after (D) exposure to isoproterenol. (E) Comparison of average values of $\Delta F/F_0$ and I_{NCX} in each group (*$p < 0.05$, **$p < 0.01$). (F and G) Effects of isoproterenol on spontaneous Ca^{2+} release activity in regularly depolarized (0.2 Hz) dialyzed with pipette solutions containing 5 or 15 mM Na^+. (F) Changes in Ca^{2+} transients (Fluo-4), I_{Ca} and I_{NCX} at the onset of exposure to 100 nM isoproterenol in mutant iPS-CM (NP0014-C1) dialyzed with 5 (top) or 15 mM Na^+ (bottom). (G and H) Effects of isoproterenol on baseline Ca^{2+} (F_0, Panel G) and the fraction (in %) of cells with spontaneous Ca^{2+} releases (intervening between the I_{Ca}-triggered transients; Panel H) of control (WT) and mutant (NP0014) biPS-CM) dialyzed with 5 or 15 mM Na^+ before and after exposure to isoproterenol. The numbers of examined cells are shown in parentheses.

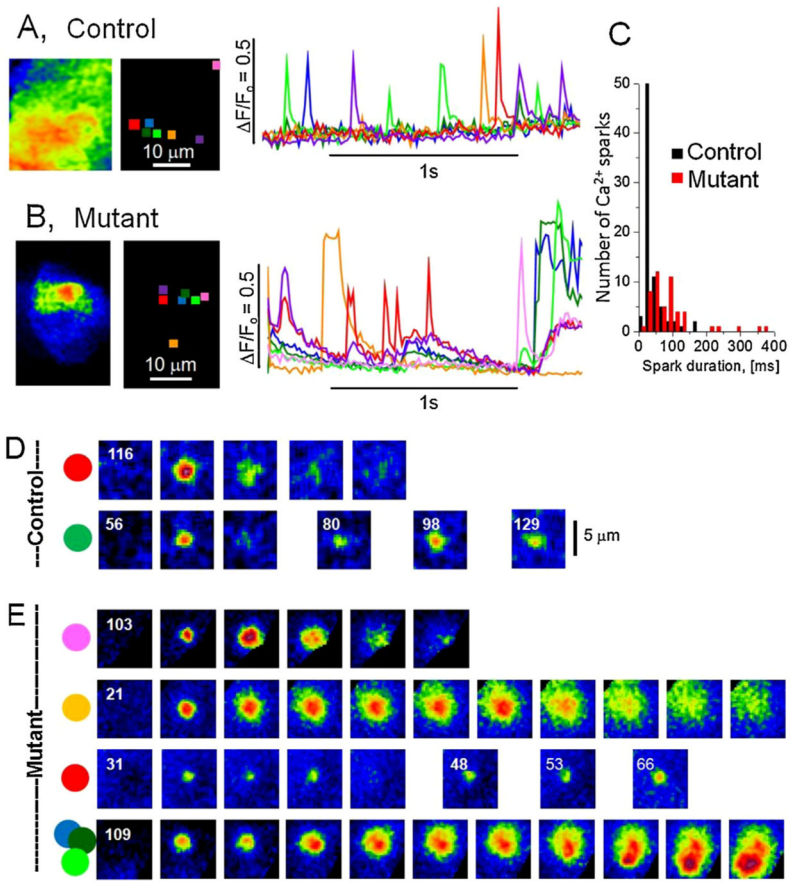

Fig. 7.

Ca^{2+} sparks in control (A and D) and mutant (B and E) iPS-CM. (A and B) From left to right the panels show: (1) Images of average diastolic fluorescence distributions, (2) color coded regions of interests corresponding to locations of Ca^{2+} sparks, and (3) the time course of the normalized fluorescence intensity at these locations. The histogram in Panel C shows the distributions of the duration of Ca^{2+} sparks measured at half peak amplitude for control cells (black, average = 40.4 ± 3.5 ms, n = 76) and mutant cells (red, average = 89 ± 7.5 ms, n = 50). (D and E) Image sequences showing the evolution of Ca^{2+} sparks. The colored labels correspond to the traces in Panels A and B.

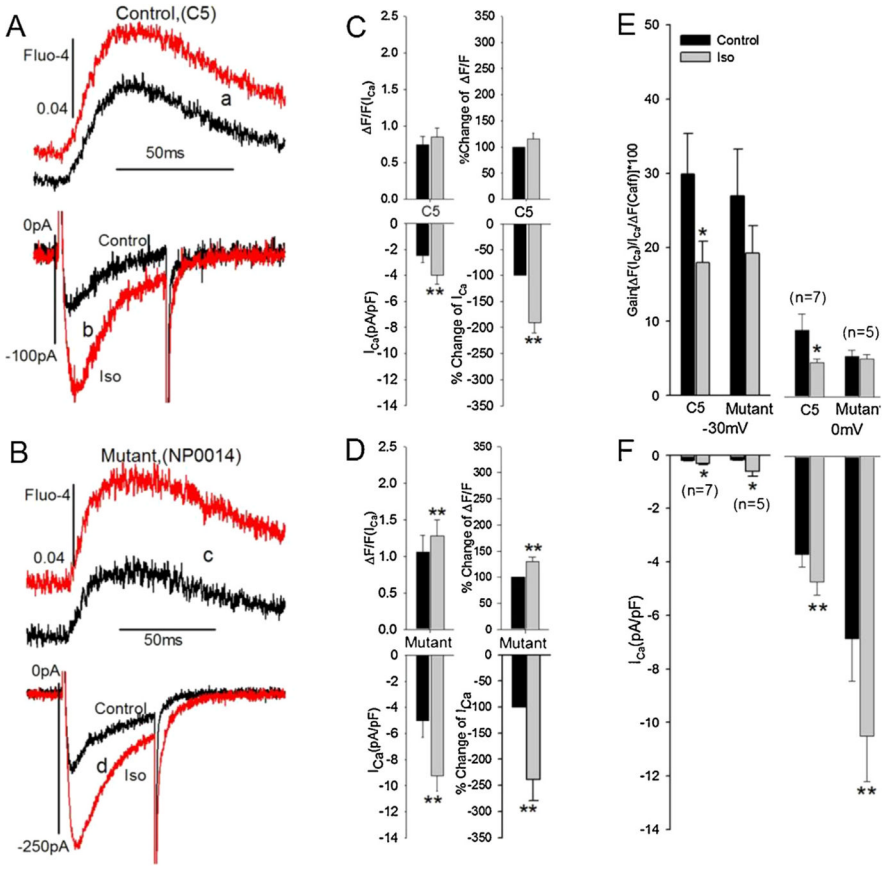

Fig. 8.

Effects of adrenergic stimulation on I_{Ca}, Ca_i-transients, and gain factor in control and mutant iPS-CM. (A and B) I_{Ca} traces and the corresponding Ca^{2+} fluorescence in control and mutant iPS-CM before (lack) and after (red) treatment with Isoproterenol. Cells were depolarized from −40 mV to 0 mV. (C and D) Average values of peak I_{Ca} and $\Delta F/F_0$ in each group before and after exposure to isoproterenol. (D and E) Effects of isoproterenol on the gain factor at −30 and 0 mV. (For interpretation of the references to color in this figure legend, the reader is referred to the web version of the article.)

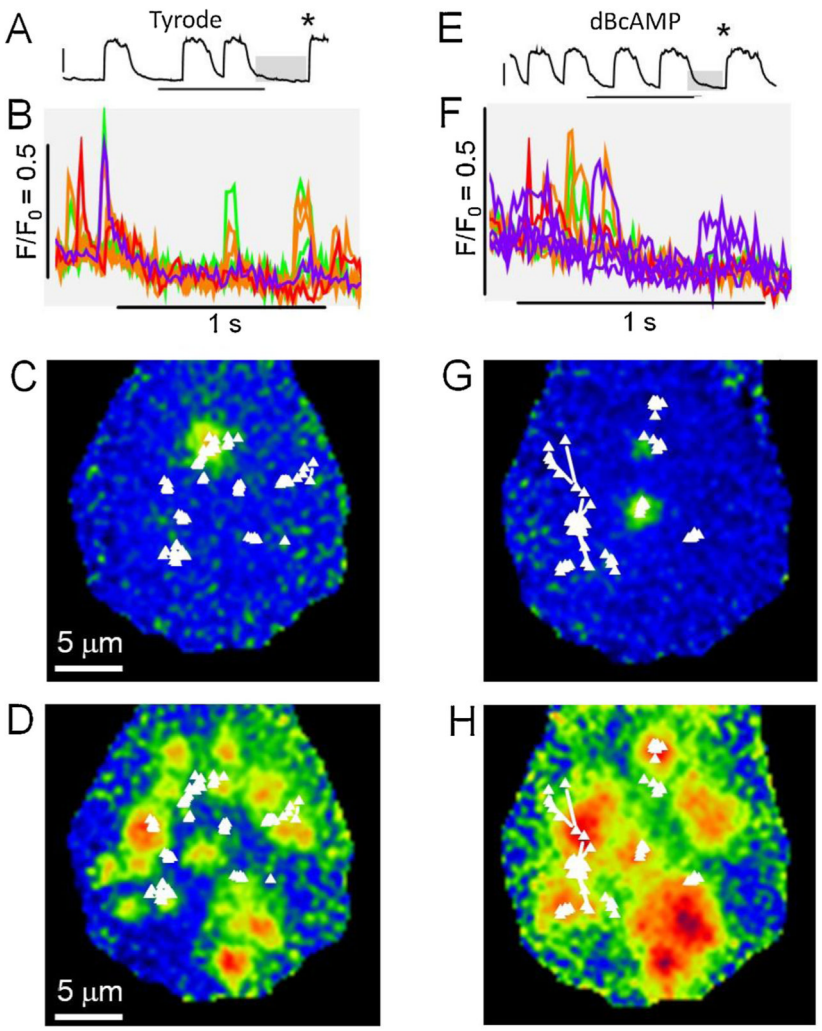

Fig. 9.

TIRF imaging of Ca^{2+} sparks in mutant iPS-CM before (A–D) and after (E–H) 3 min exposure to 100 μM dBcAMP. From top to bottom the matched panels show: The time course of cellular Ca^{2+} transients (A and E), Ca^{2+} sparks at selected color coded sites (during the diastolic interval showed in gray above, B and F), and maps of the locations of Ca^{2+} sparks superimposed on sample ratiometric images of Ca^{2+} sparks (C and G) or the onset of Ca^{2+} release (D and H at the times indicated by *s in A and E). Connecting lines show movements of the center of release from one frame to the next.

Table 1

Comparison of baseline Ca^{2+} signaling parameters and the effects of adrenergic stimulation in control and mutant iPS-CM. The upper part of the table shows a comparison of Ca-signaling parameters in control and mutant iPS-CM while the lower part shows the effects of adrenergic stimulation in each of these two groups.

	Control iPS-CM	**F2483I mutant iPS-CM**	
I_{Ca} density (pA/pF)	8.5 ± 1.3	8.6 ± 1.0	← →
Fractional Ca^{2+} release	0.26 ± 0.05	0.4 ± 0.09	← →
SR Ca^{2+} stores			
$\Delta F/F_0$ (Caff)	6.3 ± 1.0	2.7 ± 0.5	↓
I_{NCX} (pA/pF)	2.13 ± 0.27	1.32 ± 0.13	↓
CICR gain			
−30 mV	12.7 ± 2.5	21.5 ± 2.5	↑
0 mV	3.8 ± 0.7	4.4 ± 0.5	
Ca^{2+} sparks	Short and sporadic	Longer and wandering	
Adrenergic stimulation			
ΔI_{Ca}	% 90.6 ± 19.6 * ↑	% 138.8 ± 40.3 * ↑	
CICR gain			
−30 mV	30–18 * ↓	27–19 *	
0 mV	9.0–5.0 * ↓	5.4–5.1	
Diastolic Ca^{2+} (F_0)			
5 Na^+_i	0.13–0.14 * ↑	0.1–0.13 * ↑	
15 Na^+_i	0.18–0.19 * ↑	0.17–0.2 * ↑	
% increase in # cells generating spontaneous Ca^{2+} release			
5 Na^+_i	3% ↓	9% ↑	
15 Na^+_i	18% ↑	24% ↑	

* indicates significance at the $p<0.05$ level.